Journal of Nepal Geological Society, 2013, Vol. 46, pp. 57-68

The formation mechanism of garnet porphyroblast in quartz schist, Namche Barwa, east Himalaya

Zhihui Cai[1,2] and *Hui Cao[1,2]

[1]State Key Laboratory of Continental Tectonics and Dynamics, Institute of Geology, Chinese Academy of Geological Sciences, Beijing 100037, China
[2]Institute of Geology, Chinese Academy of Geological Sciences, Beijing 100037, China
*(*Email:caohuicags@gmail.com)*

ABSTRACT

The quartz schist in the Indus-Yarlung Tsangpo suture zone, from Namche Barwa, east Himalaya undergone extensive mylonization with well developed foliation and lineation; its S-C fabric, "σ" and "δ" type porphyroblasts and asymmetrical folds indicate the northwestward normal slip ductile shear deformation. The electron backscattered diffraction (EBSD) data, lattice preferred orientation (LPO) patterns for quartzes in the matrix foliation (or external foliation, S_3) and inclusion-trails in the rim of the garnet porphyroblasts (S_2) both show a top-to-NW (normal) shear sense. While LPO patterns for quartzes of the inclusion-trails in the garnet porphyroblast cores (S_1) show an opposite shear sense (top-to-SE). The garnet compositional zonation indicates a growth zoning characteristic from energy dispersive spectroscopy (EDS) analysis. By connecting the inclusion-trails in garnet cores, an initial foliation trace with asymmetrical fold shape can be obtained. It suggests that these garnet porphyroblasts with snowball structure formed on the asymmetrical folds by the rotation of external shear sense rather than the rotation of garnet porphyroblasts. Garnet porphyroblast with snowball structure proposed that the rocks from the Indus-Yarlung Tsangpo suture zone west side of the Namche Barwa syntaxis have undergone southeastward thrusting and later followed by northwestward normal slipping.

Key words: Garnet porphyroblasts, EBSD, snowball structure, Indus-Yarlung Tsangpo suture

Received: 30 October, 2012 **Revision accepted**: 14 June, 2013

INTRODUCTION

Garnets in metamorphic rocks record both metamorphic and deformation processes. It is composed of 8 molecules totaling 150 atoms molecular, with a formula $A_3B_2[SiO_4]_3$, where A stands for bivalent cation ions like Mg^{2+}, Fe^{2+}, Ca^{2+} or Mn^{2+}; B for trivalent cation ions like Al^{3+}, Fe^{3+} or Cr^{3+}. Garnet composition necessitates high temperatures and long durations for the bulk diffusion of both principal- and micro-elements. This implies that both the growth and diffusion of garnet may be viewed as a nearly closed system. This characteristic has been widely used to understand the crustal evolution of the metamorphic rocks in the core of an orogeny (Mezger et al. 1989; 1992; Burton et al. 1995; Ganguly et al. 1998; Erik et al. 2000; Carlotta and William 1999; Caddick et al. 2010). Garnet is more protective for some radioactive elements than its host rocks. Therefore it is an ideal mineral for radioactive dating. Garnet is involved in many reactions relating to temperature and pressure due to variation of Ca-Mg-Fe-Mn solid solutions. Therefore it is widely applied to geological temperature or pressure measurement. The nucleation, growth, metamorphic process and rheology of garnet have also become a hotspot for geological researches (Steinhardt 1989; Toshiaki and Sachiyo 1989; Ando et al. 1993; Ji and Martignole 1994; 1996; Den Brok and Kruhl 1996; Ji et al. 2003; Williams and Jiang 1999; Brecht et al. 1996; Kleinschodt and McGrew 2000; Mainprice 2004). The substantial development in high temperature/pressure experiment, transmission electron microscope (TEM), electron backscatter diffraction (EBSD) and the penetration of other sciences into the geological world have provided us with better understanding of garnet behavior in multiply deformed rocks (Steinhardt et al. 1989; Ji et al. 1994, 2003; Williams et al. 1999; Prior et al. 2002; Mainprice 2004; Storey and Prior 2005).

Attempts have been made on the formation mechanism of garnet porphyroblasts. It is the focus of extensive research over the past two decades on whether rotation took place in garnet porphyroblast or not during orogenic deformation and metamorphism. Some researchers have numerically simulated on computer the formation process of garnets with snowball structure. These numerical simulations include two-dimensional digital simulation by Toshiaki and Sachiyo

Paper presented in 27th HKT Workshop, Kathmandu, Nepal, 28-30 Nov., 2012

(1989) and three-dimensional digital simulation by Stallard and Hickey (2001), Passchier et al (1992) and Evins (2005). Normal digital simulations by these researchers show that rigid garnet porphyroblasts generally rotate with the shear flow of the matrix in the course of rock deformation or metamorphism. However, many think completely differently as to whether garnets with snowball structure rotated during their formation. For example, Aerden (1995) and Jung et al (1995) suggest that the rotation involved in the formation of porphyroblasts with snowball structure is the shear sense of the matrix rather than the rocks themselves. Jung et al (1999) reported nearly the same direction of the core foliation S_1 among different garnets, which they took as grounds that the garnet porphyroblast in their samples had not rotated. Bell (1981; 1985; 1989) argues that porphyritic crystals do not rotate when the substance being deformed is heterogeneous enough to decompose the deformation and will have to rotate during progressive simple shear processes when the deformation is not decomposed, in which case there is only a progressive shear component other than a shortening one.

In this paper, kinematic and dynamic studies are carried out on the nucleation, growth and deformation of garnets with snowball structure from the quartz schist in Indus-Yarlung Tsangpo suture zone, Milin, Namche Barwa area, Tibet. Using microscopic observation, energy dispersive spectroscopy (EDS) and electron backscatter diffraction (EBSD), in combination with the regional metamorphism and deformation record, and on this basis, the indicative implications of these garnets with snowball structure for the tectonic evolution of Indus-Yarlung Tsangpo suture zone are discussed.

REGIONAL GEOLOGY AND DESCRIPTION OF SAMPLES

The gigantic Himalayan orogen (about 2500 km long) E–W trending, southward-protruding (Fig. 1a) is regarded as the northern margin of Indian plate, bounded by the main front thrust in the south, Indus-Yarlung Tsangpo suture zone in the north. To the east and west it terminates at both ends in syntaxis (Wadia 1931). The eastern syntaxis (Namche Barwa syntaxis) is the east extension of the Greater Himalayan crystalline complex which is the metamorphic core of the Himalayan orogen (e.g., Le Fort 1996; Yin and Harrison 2000; Yin 2006; Guillot et al. 2008) (Fig. 1a). The Indian continent has its eastern corner wedged northeastward into the Lhasa terrane with a "Ω" shape, on the boundary of which occurs the Indus-Yarlung Tsangpo suture (Fig. 1b). The Namche Barwa syntaxis contains of reworked pre-existing Proterozoic rocks (Pt_z and Pt_p in Fig. 1b, d) and Duoxiongla massif (marked by leucocratic granite, migmatite and widespread ductile deformation.) (Fig. 1b, d) with peak metamorphism (1.7–1.8 GPa, 870–897°) (Zhong and Ding 1996; Liu et al. 1998). The Indus-Yarlung Tsangpo suture at Milin, Namche Barwa area is consisted of typical ophiolites and mélange system, of which quartz schists are the most principal part that constitutes the matrix of the melange zone together with green schists (transformed from basalts) (Zhong et al. 1996). Quartz schists include kyanite-mica-feldspathic quartz schists, garnet-mica quartz schists, garnet-kyanite-mica quartz schists and mica quartz schists. Their primary rocks might have been clay-rich siliceous rocks and sandy or argillaceous rocks close to continents or island arcs (Geng et al. 2004).

Deformation along the Indus-Yarlung Tsangpo suture zone shows variations from place to place (Xu et al. 2012). The southern segment in Milin area is a N–S or NE–SW trending, normal shear zone with down-dip stretching lineation (Fig. 1c). Our samples, V3-1, V3-2, V3-3 and V4-1, were collected from different outcrops in Milin in the Indus-Yarlung Tsangpo suture, Namche Barwa (Fig. 1b, 1c). Fig. 2a shows the field photos of sample V3-1, which present noticeable overall deformation of the rock. This is more serious in sample V4-1, where many tiny folds are observed. The foliation dips to NW. The S-C fabric, "σ" and "δ" shape porphyroblasts and asymmetrical folds implicate a top-to-NW shear movement.

METHODOLOGY

Samples were collected perpendicular to the foliation (XY) and parallel to the lineation (X) (Fig. 2b) to view their texture, structure and mineral category. Oxford energy dispersion spectrometry (EDS) was used to test the mineral components at the working voltage of 20 kV, using Co pure metals and silicate minerals as the standard samples. J EOL JSM-5610 scanning electron microscope was used to view the backscatter electron images of the samples. EBSD was used to measure the fabric of the garnet. The working principal of EBSD is to place a fine polished sample in the scanning electron microscope at a high angle (approximately 70°), where the electron beams hit on the surface of the sample and result in Kikuchi strips, each of which corresponds to a group of crystal planes. Electron backscatter diffraction pattern (EBSP) is used to identify the spatial orientation of the crystals tested, while the data are processed on CHANNEL 5 (Schmidt and Olesen 1989). The whole test was carried out in the Institute of Geology, Chinese Academy of Geological Sciences.

RESULTS

Microstructure of the quartz schist

Quartz schist samples V3-1, V3-2 and V3-3 are

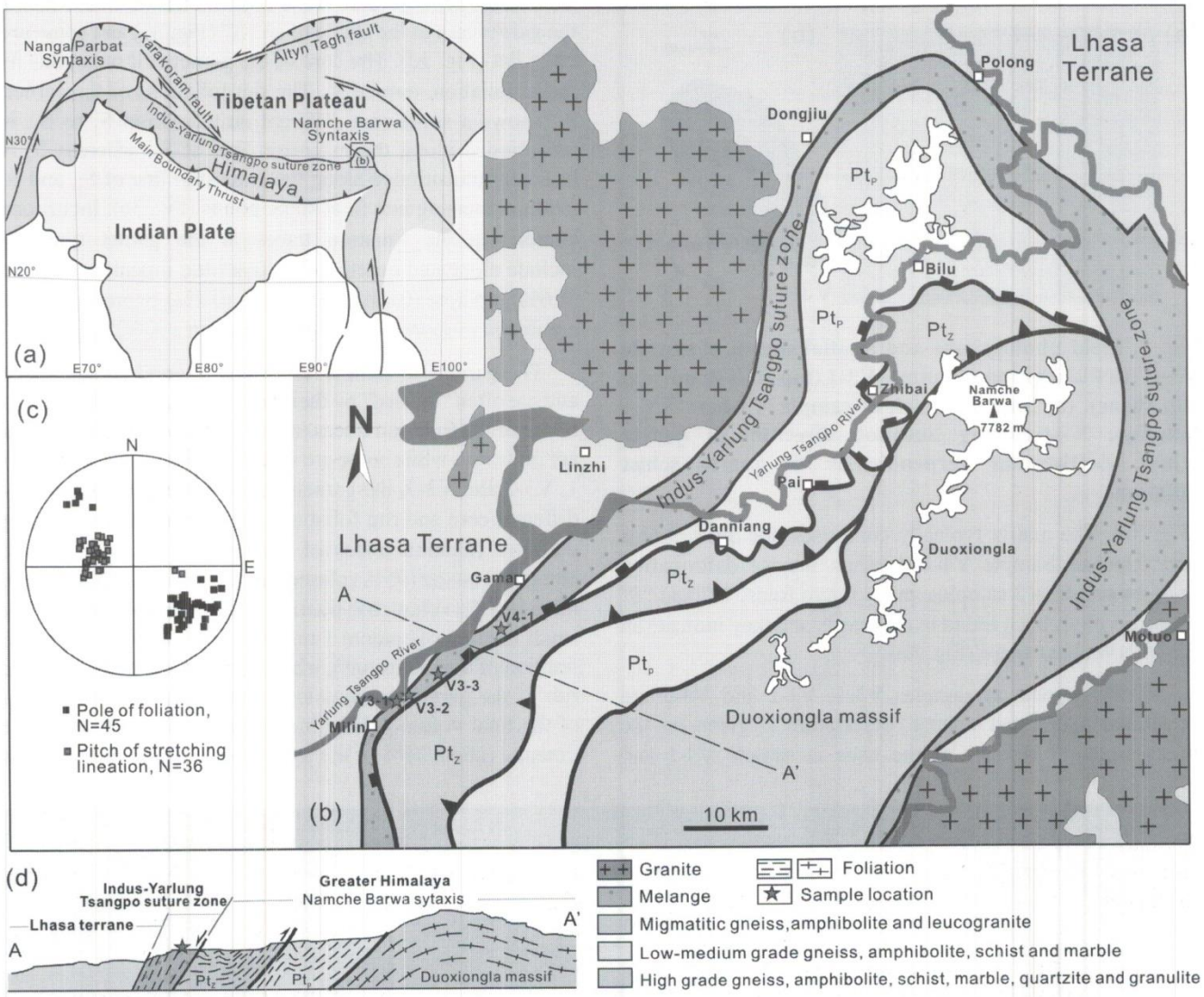

Fig. 1: (a) Simplified tectonic map the Himalayan orogen and its adjacent region. (b) Simplified tectonic map for the Milin region of Namche Barwa, East Himalaya after Xu et al., 2012, modified. (c) Lower hemisphere projection for stretching lineation and pole of foliation; (d) A NW-SE cross section (A-A') traversing the Indus-Yarlung Tsangpo suture zone.

porphyritic-lepidoblastic texture, gneissic structure of medium sizes composed of quartz (55%), feldspar (10%), muscovite + biotite (30%) and garnet (5%), plus a little proportion of ilmenite, rutile, titanite and epidote (Fig. 3a is photomicrograph of sample V3-1). Garnets porphyroblasts are slightly rigidly fractured and have snowball structure. Both hexagonal and elliptical shaped garnets were observed in these rocks (Fig. 3a). The elliptic elongation of garnets in high-grade metamorphic rocks is often construed as the result of plastic deformation or oriented growth (Ji and Martignole 1994; Ji et al. 2003), whereas elongated monocrystalline garnets in low-grade ones often relate to selective solution-sedimentation (Brecht et al. 1996). The matrix around the garnets mainly consists of quartz, mica and a little feldspar that come in very fine sizes and constitutes an asymmetrical porphyroblast system together with the garnets.

Sample V4-1 is also quartz schist, with porphyritic – lepidoblastic texture, gneissic structure of medium sizes, composed of quartz (58%), feldspar (8%), muscovite + biotite (27%) and garnet (6%), plus a little proportion of ilmenite (about 0.5% of the total rock) (volumetric fraction, with ilmenite inclusions accounting for 5% of inclusions in the garnet (volumetric fraction), rutile, titanite and epidote

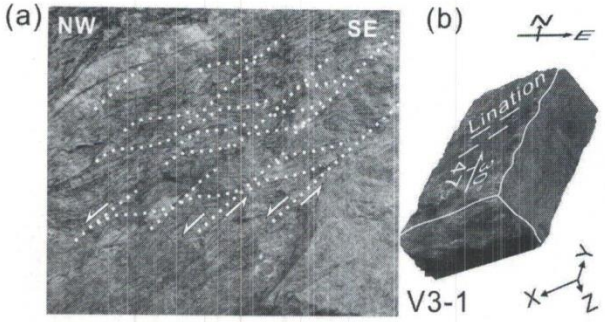

Fig. 2: Field photographs and Spatial sketch of sample V3-1. (a) Field photo of sample V3-1 (top-to-NW normal slip shear). (b) Spatial sketch of sample , where XY – foliation, X–stretching lineation direction of quartz schist, Z–Direction perpendicular to quartz schist foliation.

(Fig. 3b). The matrix typically comprises fine quartz, mica and feldspar. Sample V4-1 presents intense deformation than the previous 3 samples: many micro folds, "σ" and "δ" shape porphyroblast found in the matrix and they indicate an SE-to-NW shear sense (Fig. 3b).

As the garnets in samples V3-1, V3-2 and V3-3 are of similar shape and texture, description is given on the microstructural features of the ones in sample V3-1 and V3-2 (Fig. 3c, d), where some of the foliation traces inside the garnets are in the shape of an "S" (Fig. 3c) and some are quite flat (Fig. 3d). The core of the garnet still maintains its initial foliation, termed S_1. The rim foliations of the garnet, S_2, shows a somewhat different attitude from S_1 to S_2, is transitioned along the extension line of S_1, whereas S_3 is basically transitioned along the extension line of S_2, and S_3 is found incising into S_2 at some points (Fig. 3c). Inclusions comprising the foliation traces in the garnet typically include elongated quartz (97.2%), a little ilmenite + titanite (1.6%), epidote (0.4%) and apatite (0.4%) byproducts. The combined proportion of feldspar and mica is 0.2%.

The garnets in sample V4-1 have a good crystal shape and are often "incised" by their neighboring mica (Fig. 3e, f). Some of the foliation traces inside the garnet porphyroblasts are quite flat, while some are sigmoidal. Unlike samples V3-1, V3-2 and V3-3, the garnets in V4-1 present significantly different core and rim foliations, and inclusions comprising the core foliation traces of the garnets typically include elongated quartz (95% volumetric fraction of the inclusions), ilmenite (5% volumetric fraction of the inclusions) and a very small fraction of epidote + titanite + mica (0.5% volumetric fraction of the inclusions), whereas the foliation traces at the rim of the garnet contains less quartz (approximately 25% of the total volume of the inclusions at this part) but more ilmenite (about 75% of the total volume of the inclusions at

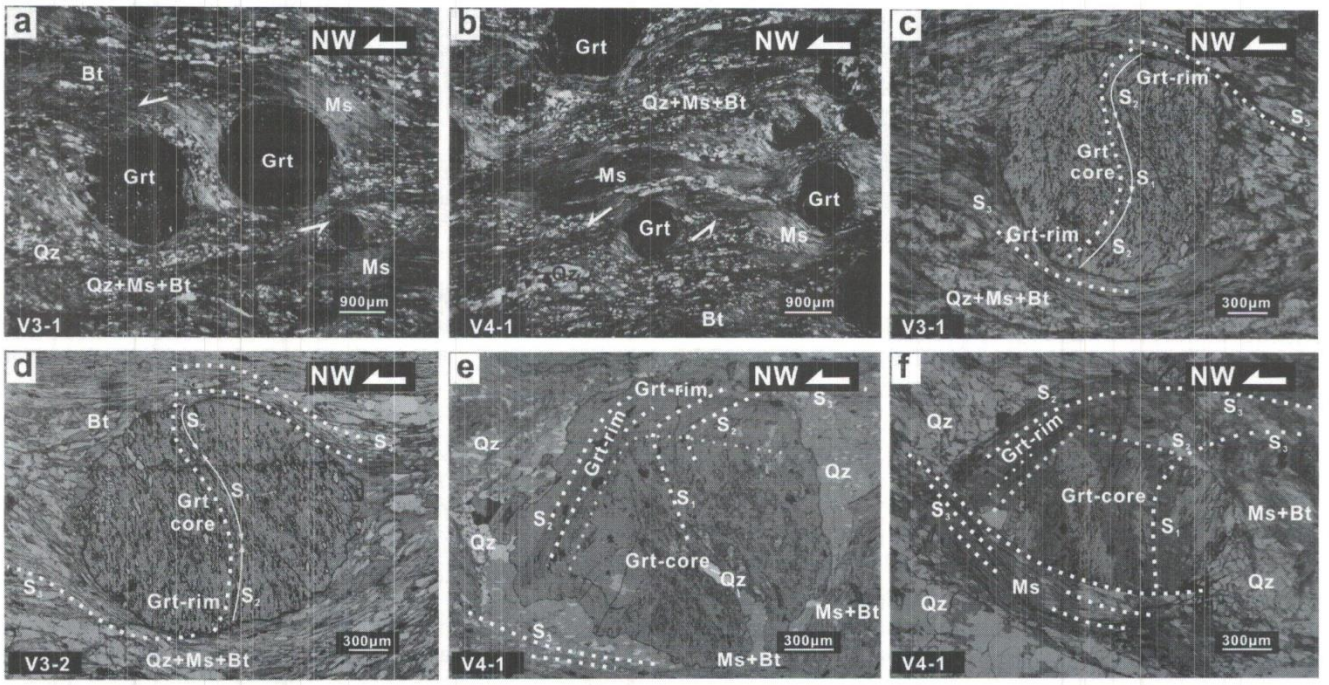

Fig. 3: Photomicrographs of mica schists from the Milin area. (a) Sample V3-1, mica quartz schist. (b) Sample V4-1, mica quartz schist. (c, d) Garnets in V3-2. (e, f) Garnets in V4-1; Grt-rim –Rim of garnet; S_1 –Stage 1 foliation; S_2 –Stage 2 foliation; S_3 –Stage 3 foliation; Grt –Garnet; Qz –Quartz; Ms –Muscovite; Bt –Biotite; Grt-core –Core of garnet.

this part) (Fig. 3e, f). The backscatter electron (BSE) images of the garnets (Fig. 4d) also demonstrate higher ilmenite content and an arrangement under a certain rhythm. The major axis of the ilmenite is parallel to the crystal boundary of the garnets. The garnets have somewhat different foliation attitudes at the core, the rim and in the matrix. The initial foliation at the core of the garnets is termed S_1, that at the rim S_2, which is transitional with S_1 along the extension line of S_1 and generally parallel to flat particle boundaries of the garnets, and that in the matrix S_3. Normal to the S_1 and S_2 traces, S_3 is transitional to S_2 (Fig. 3e, f), while obviously incises S_2 at other points (Fig. 3f).

Fabric of the garnet

Fig. 4 shows BSE images (Fig. 4a, d) and EBSD lattice orientation measurements of the garnets with snowball structure in sample V3-1 and V4-1 (Fig. 4b, c, e, f, g), where the Euler angle distributions of 16 511 measuring points at different points of the same garnet are in the same color (black parts in Fig. 4c), implicating the same garnet lattice orientation among different measuring points (Fig. 4c); the lower hemispherical projections of almost all the 16 511 measuring points fall at the same point (Fig. 4b), suggesting the lattice has not undergone any significant deformation or distortion, and there have been no linear dislocations or planar defects inside the crystal, such as kinks, twin crystals or subgrain boundaries. The same is presented in the fabric diagrams, and by the measurements of the garnets in Sample V3-2 and in V3-3, where the same spatial orientation is maintained at different points of the same garnet. EBSD measurements indicate that while in analysis samples V3-1, V3-2 and V3-3, the garnet contains curved inclusion traces, but these have not resulted in changes in the lattice orientation, and the garnets have not undergone plastic deformation.

EBSD surface scanning test of the garnets in sample V4-1 indicates a different color at the core (black) from the rim (grey) in the Euler angle distribution map of the same garnet, suggesting certain azimuth angle difference between measuring points at the core and those at the rim (Fig. 4f). Fig. 4g shows the EBSD images of the azimuth angle difference between adjacent measuring points, where the red means the azimuth angle difference between adjacent measuring points is 3°, while blue means the difference is 10°. No obvious red or blue line is shown between the core (Grt-core) and the rim (Grt-rim), indicating the azimuth angle difference presented in Fig. 4f is smaller than 3°.

An EBSD surface scanning fabric test was conducted at the core-rim interface of the garnets in V4-1, and indicates slight difference in the fabric diagrams obtained at 6 069 measuring points at different parts of the garnet (Fig. 4e).

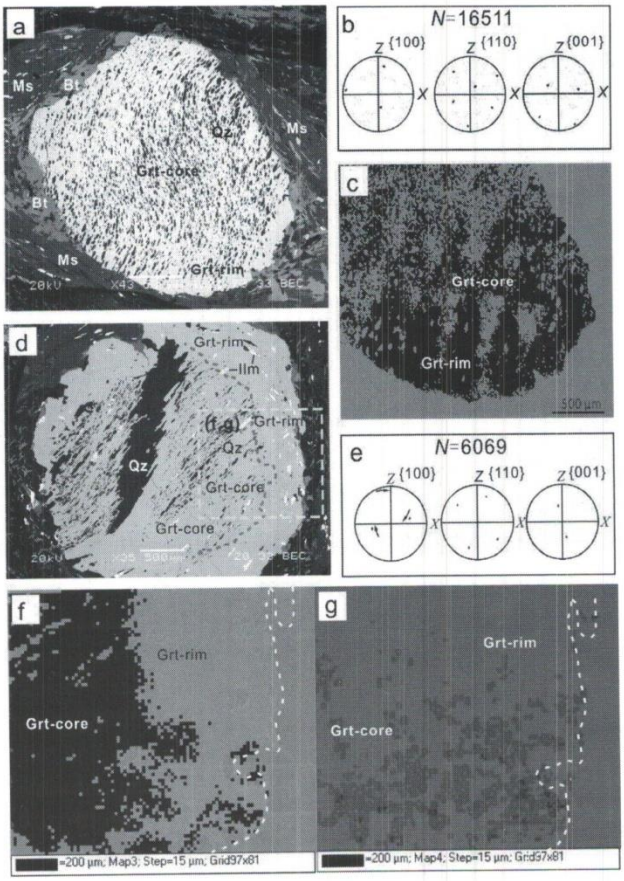

Fig. 4 Text of garnet with snowball structure in the sample V3-1 and V4-1. a, d –Backscatter electron (BSE) image of garnet; b, e –Fabric diagram of garnet; c, f –Euler angle distribution diagram of garnets corresponding surface scanning area are presented in figure a and d, the black and grey parts are garnet, the green parts are other mineral than garnet, the different colors indicate the difference in the azimuth angle; g –Azimuth angle difference distribution between adjacent measuring points, where the red is 3° and the blue is 10°; XY – Foliation, X –Stretching lineation direction of quartz schist, Z –Direction perpendicular to stretching lineation of quartz schist, N –Number of measuring points; Grt-core: garnet core; Grt-rim: garnet rim.

This also suggests the azimuth angle difference between the core and the rim of different garnets.

Compositional zonation of the garnet

Compositional analysis of the garnets in samples V3-1, V3-2, V3-3 and V4-1 shows a decline in the Ca and Mn contents, and a significant increase in the Mg and gradually increase Fe contents from the core to the rim for all the garnets (Fig. 5), indicates a growth zoning feature.

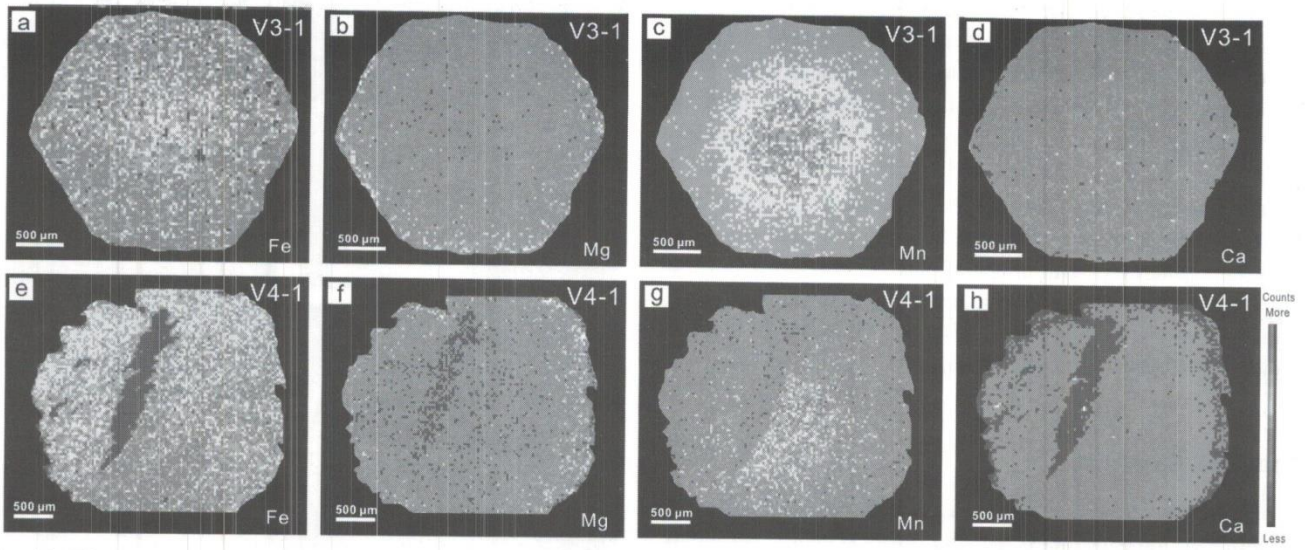

Fig. 5: Element maps of garnets from mica schist samples V3-1 and V4-1. The garnets show significant chemical zoning with decreasing Fe(a, e), increasing Mg (b, f) and decreasing Mn (c, g) and Ca (d, h) indicating growh zoning; a~d– Element maps of a garnet in sample V3-1; e~h– Element maps of a garnet in sample V4-1.

Quartz fabric in the matrix

The quartz fabrics in the matrix of samples V3-1, V3-2, V3-3 and V4-1 showed an SE-to-NW normal slide shear (Fig. 6a), which is consistent with microscopic structural features (Fig. 3a). XY means the foliation in matrix, S_3; X is the axis parallel to the stretching lineation; Z is the axis perpendicular to the foliation.

Quartz inclusion fabric in the garnet

Garnet porphyroblasts with snowball structure were randomly selected from samples V3-1, V3-2, V3-3 and V4-1, to test the mineral fabrics in their quartz inclusions by EBSD surface scanning. In Fig. 6b ~ k, XY stands for the quartz foliation; X the direction parallel to the stretching lineation; Z-axis the direction perpendicular to the mylonite foliation; X′Y′ the foliation in the garnet formed by oriented arrangement of inclusions; X′-axis the direction parallel to the tangent of the curved foliation traces; Z′ the direction perpendicular to the X′Y′ foliation. The longitudinal direction of the initial coordinate of the fabric diagrams obtained by EBSD testing is the Z-axis, and the horizontal direction is the X-axis. By measurement, the angle between the X-axis and X′-axis will be obtained. By rotating the reference coordinate system according to this angle, we may turn the longitudinal direction to be the Z′-axis, the horizontal the X′-axis, leaving the Y-axis unchanged. By re-projecting in the new coordinate system, the quartz fabric diagram at the measuring point will be obtained. This is how we obtained all the following fabric diagrams of the quartz inclusions in the garnets (Fig. 6b ~ k).

Fig. 6b and Fig. 6c shows photos of garnets I and II in sample V3-1 under a mono-polarized microscope, where the inclusion trace curve in garnet I is quite flat and is 62° from the quartz schist foliation; the inclusion traces in garnet II take the shape of an "S", with the core 97° from the quartz schist foliation XY, and rim inclusion traces 145° from the quartz schist foliation. We tested garnet I in sample V3-1 (including the core and the rim) by EBSD surface scanning and obtained 12 538 measuring points on the quartz. The c-axis lower hemisphere projection density is 3.02 maximum and 0.44 minimum, which means the difference between the maximum and the minimum density is quite limited, suggesting comparatively decentralized projection and insignificant lattice preferred orientation (Fig. 6b I-whole). The quartz measuring points obtained at the core of the garnet, however, total 3 249, which enabled us to obtain more centralized c-axis projection density diagrams, Fig. 6b I-core presents a noticeable top-to-SE tendency, compared to the garnet rim that is typically top-to-NW (measuring point number N = 2 625) (Fig. 6b I-rim). Garnet II was tested by EBSD surface scanning, which resulted in 9 201 quartz measuring points, with the c-axis lower hemisphere projection density being a merely 2.33 maximum and 0.32 minimum, which means quite decentralized projection, suggesting that more than one fabric pattern might have been involved (Fig. 6c II-whole). The quartz fabric diagram at the core of garnet II is similar to that of garnet I, i.e., both bear a top-to-SE shear sense (Fig. 6c II-core). Fig. 6c II-rim is the c-axis lower hemisphere projection at the rim of the garnet, which is top-to-SE, at the measuring points of 1 429. Besides, we also measured the fabric of quartz inclusions

in other 4 garnets in sample V3-1 and resulted in much the same mineral fabrics as those in the 2 garnets: top-to-SE at the core and top-to-NW at the rim.

Garnets with snowball structure in sample V3-2 have similar fabric characteristics to those in V3-1. Fig. 6d ~ f show microscopic images of 3 garnets in sample V3-2 and their fabric diagrams. The quartz inclusion trace of grain I is a flat "S" shape that of grain II is an "S" shape, while that of grain III is comparatively flat. The quartz inclusion measuring points from whole surface scanning of garnet I total 1 500, without a definite preferred orientation (Fig. 6d I-whole), whereas the core and the rim present a top-to-SE and a top-to-NW shear sense, respectively (Fig. 6d I-core, Fig. 6d I-rim). The quartz inclusion fabric diagram obtained by whole surface scanning of garnet II does not show a definite preferred orientation either (Fig. 6e II-whole), but presents an opposite shear sense at the core to the rim; the core is top-to-SE while the rim top-to-NW (Fig. 6e II-core, Fig. 6e II-rim). The quartz inclusion measuring points from whole surface scanning of garnet III total 2 642 and present both a top-to-SE and a top-to-NW shear sense (Fig. 6f III-whole): a top-to-SE shear sense at the core (Fig. 6f III-core), and a top-to-NW shear sense at the rim (Fig. 6f III-rim).

The quartz inclusion trace in garnet I with snowball structure in sample V3-3 is slightly curved (Fig. 6g I). Whole surface scanning was conducted on the garnet. The resultant quartz measuring points total 1 893, and present both a top-to-NW and a top-to-SE shear sense (Fig. 6g I-whole); the measuring points at the core total 1 018, and the shear sense also contains both a top-to-NW and a top-to-SE component, possibly because the core scanning scope of the garnet selected was included part of the garnet rim (Fig. 6g I-core); whereas the quartz fabric diagram of rim I-rim presents a noticeable top-to-NW shear sense (Fig. 6g I-rim). The quartz

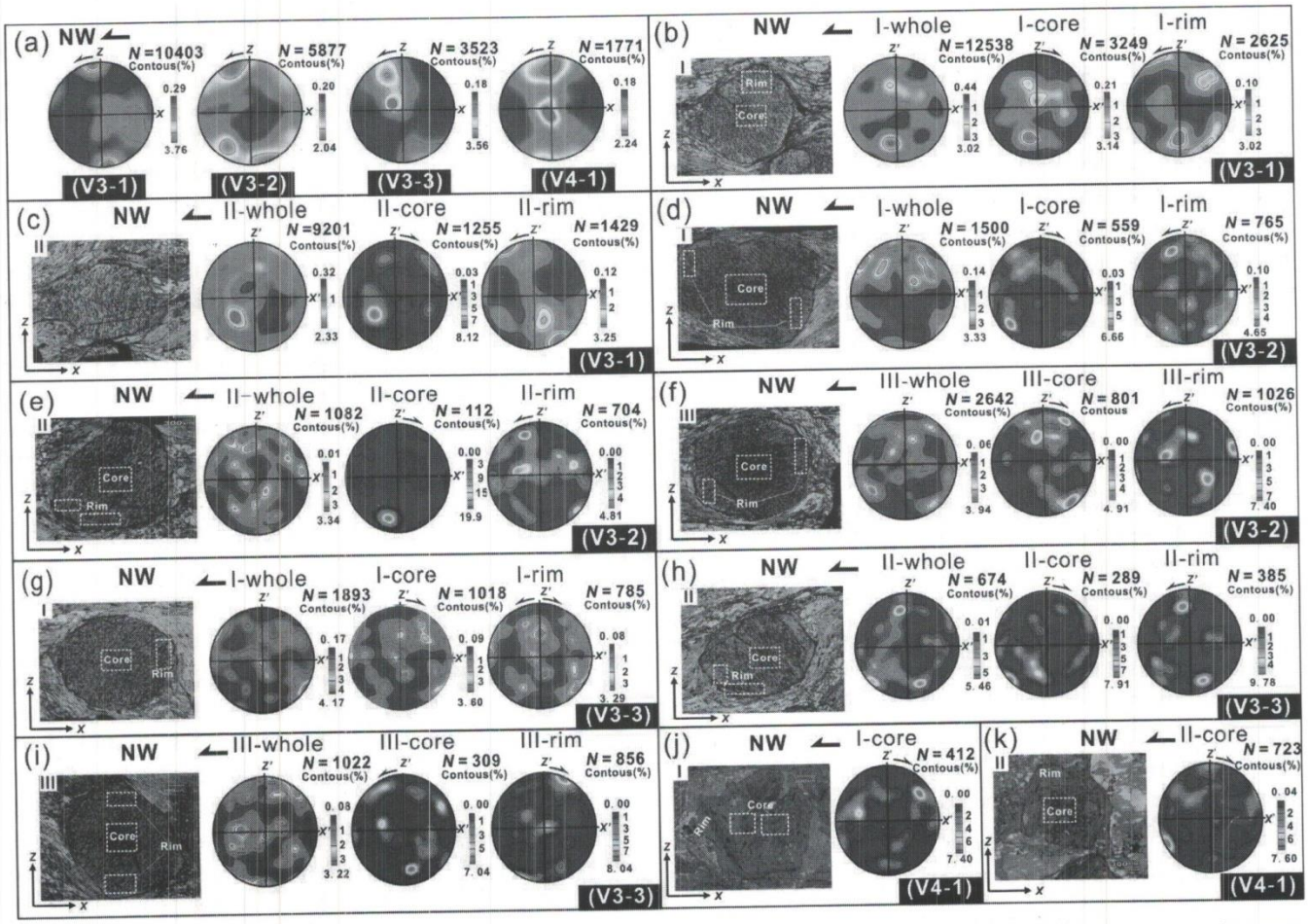

Fig. 6: LPOs of quartz in matrix and garnets. Lower hemisphere projection: X –Stretching lineation direction of quartz schist, Z –Direction perpendicular to stretching lineation of quartz schist, XY –Foliation of quartz schist, the X′-axis is parallel to inclusion trace, Z′–Direction perpendicular to inclusion foliation, N –Number of measuring points, I, II – Garnets I and II, whole –fabric diagram obtained by whole surface scanning of garnet, core –Fabric diagram obtained by scanning garnet core, rim –Fabric diagram obtained by surface scanning of garnet rim, the dashed rectangular box is the range of EBSD surface scanning.

inclusion trace of the second garnet II is quite flat (Fig. 6h II), the measuring points from whole surface scanning total 674, and present a dominant top-to-NW shear sense (Fig. 6h II-whole), while the core quartz inclusion fabric diagram (Fig. 6h II-core) presents an apparently opposite shear sense (top to SE) to the rim quartz inclusion fabric diagram (top to NW) (Fig. 6h II-rim). The quartz inclusion trace of the third garnet III is flat and presents both a top-to-NW and a top-to-SE shear sense (Fig. 6i III-whole); the core quartz fabric diagram (Fig. 6i III-core) is top-to-SE, while the rim quartz fabric diagram (Fig. 6i III-rim) top-to-NW.

The rim of the garnets in sample V4-1 contains too few quartz inclusions to serve as measuring points for fabric measurement. So we only measured the quartz inclusions at the core of the garnet in V4-1 by EBSD. The resultant quartz inclusion traces at the core of both grain I and grain II are quite flat (Fig. 6j I, k II); the quartz measuring points total 412 and 723, respectively, and both fabric diagrams present a top-to-SE shear sense (Fig. 6j I-core, Fig. 6k II-core).

In general, the quartz inclusions at the core of the garnet present an opposite shear sense to that at the rim and the matrix. The quartz at the core of the garnet presents a top-to-SE shear sense, which represents the early shear sense of the shear zone in which the quartz schist is present; the quartz both in the matrix and at the rim of the garnet presents a top-to-NW shear sense, which represents the late shear sense of the shear zone where the quartz schist is present.

Core foliation attitude of the garnet

178 garnets were selected randomly from 20 XZ sheets of samples V3-1, V3-2, V3-3 and V4-1 to measure the attitude of the initial foliation S_1 at the core. 85 garnets had their S_1 NW-inclined, many had their angle between S_1 and the quartz foliation S_3 ranging between 31 ~ 60°, totaling 42, while few had this angle larger than 60°; 93 garnets had their S_1 SE-inclined, and the angle between S_1 and the quartz foliation S_3 mostly ranged 46 ~ 90°, few had angle between S_1 and S_3 less than 45°, especially between 16 ~ 30°, only 3 garnets had this angle smaller than 10°. It means that on the XZ two-dimensional plane, angles between SE-inclined S_1 and S_3 always steeper than these between NW -inclined S_1 and S_3 (Fig. 7).

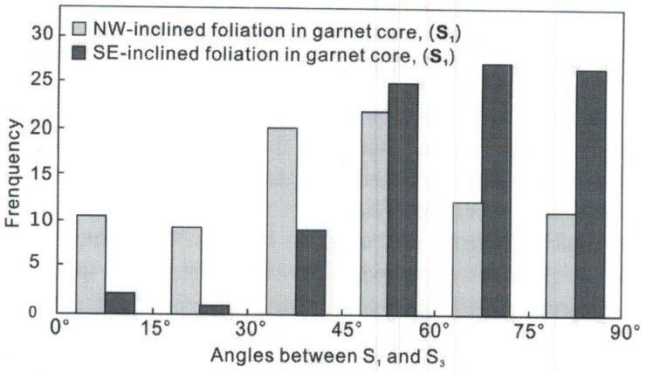

Fig. 7: Histogram of angles between S_1 and S3.

DISCUSSIONS

Formation mechanism of garnet with snowball structure

The formation of garnet with snowball structure is believed to be a process of pressure reduction and temperature increase.

Garnet zonation in metamorphic rocks not only records the growth process and balance conditions of the garnet, but also indicates the thermal history of the rock where it is present. The compositional images of the garnets in our samples indicate a declination of Mn and Ca contents, an increase of Mg and Fe contents in the garnets from the core to the rim, suggesting a typical growth zonation. As Ca and Mn contents are mainly pressure-dependent, a Ca declination and Mn increase will mean pressure reduction; as the Mg and Mg/(Mg + Fe) contents reflect temperature fluctuation, an increase in Mg and Mg/(Mg + Fe) of this study (Fig. 5) (content increase of Mg is much more significant than the Fe) mean temperature increase. So during the formation of the garnets with snowball structure we studied, the pressure reduced and the temperature increased. The Fe content gradually increased from the core to the rim. This may be explained by a possible retrogressive metamorphic diffusion, which might have been the result of exchange reaction with biotite when the rock was cooling down (Spear 1993). This process came later than the crystallization process of the garnets.

The formation of garnet with snowball structure is accompanied by fluid action

Ductile shear deformation is always accompanied by fluid action, which plays an important role in strain rate changes (Steinhardt et al. 1989). The rocks we studied are inferred to have undergone dehydration during their ductile deformation: chlorite + muscovite = garnet + biotite + quartz + water; chlorite + quartz = garnet + water; muscovite + chlorite + quartz = biotite + water. Intragranular water is the most and the strain rate reaches its highest point when the chlorite in the rock is reduced to the minimum (Williams and Jiang, 1999; Barker 1994).

Under fluid and stress actions, selective solution and sedimentation took place in garnets with snowball structure (Vollbrecht et al. 2006). They dissolved at points where there is more stress and recrystalized where the stress is less

centralized, resulting in a mica "incision" into the garnets in our samples (Fig. 3).

The formation of garnet with snowball structure might have been accompanied by plastic deformation

Samples V3-1, V3-2 and V3-3 demonstrate a lower grade of deformation than sample V4-1. Microscopic images show a transitional relation between the initial foliation S_1 maintained at the garnet core of V3-1, V3-2 and V3-3 and the rim foliation S_2 (Fig. 3c, d), whereas the initial foliation S_1 maintained at the garnet core in V4-1 is locally oblique to S_2 and does not present a significant transitional relation (Fig. 3e, f). Fabric measurement by EBSD surface scanning indicates consistent lattice orientation at all points inside the garnets with snowball structure in samples V3-1(Fig. 4b, c), V3-2 and V3-3, suggesting the formation of these garnets were not accompanied by plastic deformation, and the curved foliation traces inside them are completely the result of the garnet growth. The fabric measurement of the garnets in sample V4-1 by EBSD surface scanning(Fig. 4e ~ g), on the other side, indicates a slight azimuth angle difference between the core and the rim, which is as small as less than 3° and too small to obtain its exact value by EBSD. Karato et al (1995) demonstrated by experiments that the rheologic strength of single-grain garnets is higher than feldspar, picrite and olivine, on account of a longer Burgers vector and bcc (Body Centred Cubic Structure) accumulation. Rabier and Garem (1984) suggested garnets could be subject to plastic deformation through dislocated decomposition. Dislocated slip under high stresses is generally believed to be the direct cause of high-temperature plastic deformation in garnet facies minerals. Some experiments also indicate that slip is the main contributor to garnet deformation (Barker 1994). Doukhan et al (1994) and Ji and Martignole (1994) insisted that garnet recovery and climb in the nature are essential deformation mechanisms of garnets with snowball structure. It is possible that the plastic deformation described of the garnets with snowball structure herein is temperature and pressure-dependent, which might relate to the formation of ilmenite enriched at the garnet rim, and the dislocated creep of the garnets might took place under this temperature, which exact value we did not obtained. Besides, what was the deformation strain of the garnets with snowball structure during their formation? What is the exact plastic deformation mechanism? These are left to be further studied in the next steps.

The initial nucleation of garnet with snowball structure is superposed over an existing fold

While different garnets in our samples do not present the same attitude of the core foliation S_1, they do have a certain rule: on the XZ two-dimensional plane, the numbers of garnets whose S_1 are NW and SE-inclined are quite similar, though NW-inclined angles of 31 ~ 60° total the most, while SE-inclined angles of 61 ~ 90° totaled most (Fig. 7). Besides, EBSD testing of quartz minerals indicate the same motion sense of all the garnets when S_1 was formed: all top-to-SE (Fig. 6). If we connect the core S_1 of these garnets, we will resume a number of folds (that come in similar shapes as they have been subject to the same shear forces). These folds are asymmetrical isoclinal folds with NW-inclined axial plane, gentle NW limbs and steep SE limbs (Fig. 8a, b). We assume that the garnets with snowball structure in our samples nucleated at different points of asymmetrical folds, the inclusion traces inside the garnets took form when the shear direction changed (Fig. 8c), and the garnets themselves undergone no or very weak rotation. This coincides with the findings in Steinhardt (1989) and Aerden (1995).

Formation process of garnet with snowball structure

In the case of our samples, the formation process of garnets with snowball structure could have been (Fig. 8): (1) The rocks curved and resulted in asymmetrical folds under top-to-SE simple shearing (Fig. 8a). (2) The top-to-SE simple shear continued to act on the rocks, while in the meantime the garnets started to nucleate due to external temperature and pressure changes, and penetrative foliations S_1 occurred in rocks containing tiny garnet grains; these foliations S1 also penetrated into the garnets (Fig. 8b). While S_1 was taking form, minerals in the matrix filled in the fissures of the S_1 foliations of the garnets. As the garnets grew, these filling minerals became inclusions, and certain lattice preferred orientation occurred in these inclusion minerals (Fig. 6). (3) The shear direction changed, from thrusting to SE to normal slipping to NW. With the pre-existing internal foliations S_1, the garnets continued to grow; new minerals filled in the garnet rim normal to the S_1 foliations, and developed the same motion sense as the matrix under asymmetrical shear force, i.e. the hanging wall moved from SE to NW; the foliation at the garnet rim and in the quartz matrix at this time is the stage 2 foliation S_2. As the shear action continued, selective solution occurred in the garnets with the surrounding substances at points where there was more stress, resulting in the mica "incision" to the garnets; the foliation in the quartz rocks at this time is the final foliation S_3 (Fig. 8c).

Indication of the formation of garnet porphyroblast with snowball structure for the evolution of Indus-Yarlung Tsangpo suture, Namche Barwa and its neighboring areas

The deformation of the "Ω"-shape Indus-Yarlung Tsangpo suture in Namche Barwa varies in nature from

section to section (Xu et al. 2012). Our samples were collected from Milin at the southwest section of Indus-Yarlung Tsangpo suture in Namche Barwa, where the rocks present an top-to-NW normal slip shear sense. However, the garnet inclusions in the initial foliation S_1 maintained at the garnet core presents a top-to-SE lattice preferred orientation, which is just opposite to that displayed in the quartz at the garnet rim and in the matrix. By combining our findings with outputs from previous studies, the evolution of the Indus-Yarlung Tsangpo suture, Namche Barwa, and its neighboring areas, could be as follows.

Stage 1: The Namche Barwa metamorphic complex subduced northwestward as an antiform to below the present Indus-Yarlung Tsangpo suture closing zone (Burg et al. 1998); at points close to continents and island arcs, the primary rocks of quartz schist, siliceous rocks, deposited at small-sized marginal sea basins (Geng et al. 2004).

Stage 2: As the Namche Barwa metamorphic complex continued to subducted northwestward, relatively, the quartzites at the hanging wall suture presented an southeastward thrust. The garnets in the primary rocks of quartz schists started to nucleate. Garnets nucleate under high pressures in quartz + phengite stable areas (Geng et al. 2004). In the meantime, a top-to-SE thrust shear zone took form in the hanging wall of the northwest part of the Namche Barwa metamorphic complex. This process might have been accompanied by some shear folds and flow structures, which are partially recorded at the core of the garnets.

Stage 3: At around 50 Ma, the Namche Barwa metamorphic mass subduced to the deepest location (80 ~ 100 km, t = 800 ~ 900°C, p =2.6 ~ 2.9 GPa) (Zhang et al. 2007). Then it started to exhumate toward NE surface, and the quartzes at the hanging wall suture slipped downward in relation to the footwall. As the garnets in the quartz-schist still continued to grow, quartz inclusions formed in the garnets at this time , and present an NW preferred orientation.

Stage 4: At 10 ~ 25 Ma, the Namche Barwa metamorphic complex continued to subduce and exhumate towards SE, the late granite in the Gangdise zone in the north intruded, as products of the deep welding between the Indian plate and the Eurasian plate during the late stage of collision and orogenic period (Booth et al. 2004).

CONCLUSIONS

1. Garnets with snowball structure are the result of garnet growth under specific shear actions. The superposed nucleation of garnets took form over existing folds, possibly accompanied by lattice rotation during the formation.

2. While the Namche Barwa metamorphic complex was subducting below the Indus-Yarlung Tsangpo suture zone, and top-to-SE thrust shear zone formed at the Indus-Yarlung Tsangpo suture closing zone, producing some shear folds and flow structures at the same time. The garnets in the Namche Barwa quartz schists started to nucleate over these folds, and quartz inclusions (at the garnet core) in the garnets formed at this time present and top-to-SE shear preferred orientation. When the Namche Barwa metamorphic complex started to exhumate to SE surface, the shear direction of the shear zone at the Indus-Yarlung Tsangpo suture changed into a top-to-NW direction, with the garnets still continuing to grow. Inclusions at the garnet rim formed at this time present an NW shear sense.

ACKNOWLEDGEMENTS

This paper is supported by the National Natural Science Foundation of China (No. 40921001; 41202153), basic research funding of institute of geology, CAGS and MLR (No. J1306, J1101, 201211093) and the Geological

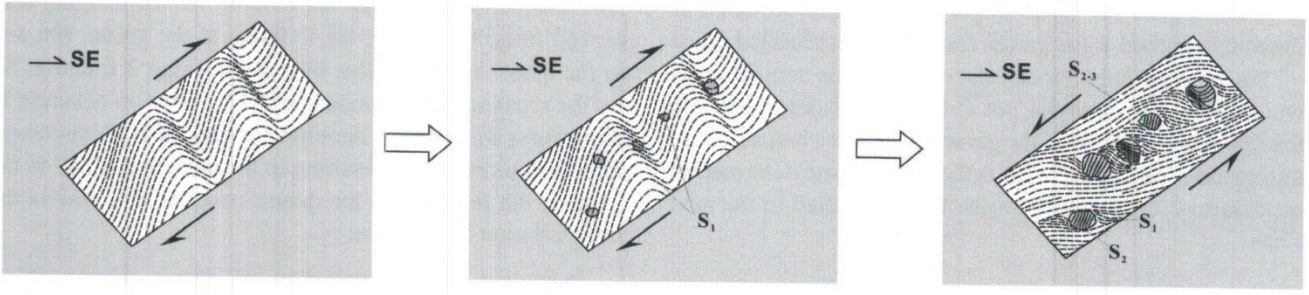

(a) Asymmetrical folds formed under top-to-SE simple shearing.

(b) Top-to-SE simple shearing continued, garnets started to nucleate , and penetrative foliations S_1 formed.

(c) Shear direction changed, top to N garnets continued to grow

Fig. 8: Model for evolution of garnet snowball.

Survey of China (No. 1212010818094). We wish to thank Academician Zhiqin Xu and Dr. Huaqi Li who offered a lot of advice and help in our compilation of this paper.

REFERENCES

Aerden, D. G., 1995, Porphyroblast non-rotation during crustal extension in the VariscanLys- Caillaouas massif, Pyrenees. Journal of Structural Geology, 1995, 17: 709–725.

Ando, J., Fujino, K. and Takeshita, T., 1993, Dislocation microstructures in naturally deformed silicate garnets. Physics of the Earth Planetary Interiors, v. 80, pp. 105–116.

Barker, A. J., 1994, Interpretation of porphyroblast inclusion trails: limitations imposed by growth kinetics and strain rates. Journal of Metamorphic Geology, v. 12, pp. 681–694.

Bell, T. H., 1981, Foliation development: the contribution. Geometry and significance of Progressive bulk inhomogeneous shortening. Tectonophysics, v. 75, pp. 273–296.

Bell, T. H., 1985, Deformation partitioning and porphyroblast rotation in metamorphic rocks: a radical reinterpretation. Journal of Metamorphic Geology, 1985, v. 3. pp. 109–118.

Bell, T. H., 1989, Johnson S E. Porphyroblast inclusion trails: the key to orogenesis[J]. Journal of Metamorphic Geology, v. 7, pp. 279–310.

Booth, A. L., Zeitler, P. K., Kidd, W. S. F., Wooden, J., Liu, Y. P., Idleman, B., Hren, M. and Chamberlain, C. P., 2004, U-Pb zircon constraints on the tectonic evolution of southeastern Tibet, Namche Barwa area. Journal of American Science, v. 304, pp. 889–929.

Brecht, M., Singer, W. and Engel, A. K., 1996, Temporal coding in the Cat Superior Colliculus. Society for Neuroscience Abstracts, v. 22, pp. 1446.

Burg, J. P., Nievergelt, P., Oberli, F., Seward, D., Davy, P., Maurin, J. C., Diao Z. Z. and Meier, M., 1998, The Namche Barwa syntaxis: evidence for exhumation relation related to compressional crustal folding. Journal of Asian Earth Sciences, v. 16, pp. 239–252.

Burton, K. W., Kohn, M. J., Cohen, A. S. and O'Nions, R. K., 1995, The relative diffusion of Pb, Nd, Sr and O in garnet. Earth and Planetary Science Letters, v. 133, pp. 199–211.

Caddick, M. J., Konopásek, J. and Thompson, A. B., 2010, Preservation of Garnet Growth Zoning and the Duration of Prograde Metamorphism. Journal of Petrology, v. 51(11), pp. 2327–2347.

Carlotta, B. C. and William, D. C., 1999, Trace element zoning as a record of chemical disequilibrium during garnet growth. Geology, v. 27, p. 555–558.

Den Brok, B. and Kruhl, J., 1996, Ductility of garnet as an indicator of extremely high temperature deformation: discussion. Journal of Structural Geology, v. 18, pp. 1369–1373.

Doukhan, N., Sautter, V. and Doukhan, J. C., 1994, Ultradeep, ultramafic mantle xenoliths a Transmission electron microscopy preliminary results. Physics of the Earth and Planetary Interiors, v. 82, pp. 195–207.

Erik, E. S., Kenneth, L. C. and Janne, B. T., 2000, Lu–Hf garnet geochronology: closure temperature relative to the Sm–Nd system and the effects of trace mineral inclusions. Geochimica et Cosmochimica Acta, v. 64(19), pp. 3413–3432.

Evins, P. M., 2005, A 3D study of aligned porphyroblast inclusion trails across shear zones and folds. Journal of Structural Geology, v. 27, pp. 1300–314.

Ganguly, J., Tirone, M. and Hervig, R. L., 1998, Diffusion kinetics of Samarium and Neodymium in garnet, and a method for determing cooling raters of rocks. Science, v. 281: 805–807.

Geng, Q. R., Pan, G. T., Zheng, L. L., Sun, Z. M., Ou, C. S. and Dong, H., 2004, Petrochemical and Metamorphic Study of Quartzite (Schist) in Indus-Yarlung Tsangpo Tectonic Zone, Namche Barwa, Tibet. Journal of Mineral Petrology, v. 24, pp. 76–82.

Guillot, S., Maheo, G., Sigoyer, J., Hattori, K. H. and Pêcher, A., 2008, Tethyan and Indian subduction viewed from the Himalayan high- to ultrahigh-pressure metamorphic rocks, Tectonophysics, v. 451, pp. 225–241.

Ji, S. C. and Martignole, J., 1994, Ductility of garnet as an indicator of extremely high temperature deformation. Journal of Structural Geology, v. 16, pp. 985–996.

Ji, S. C., Kazuko, S., Mainprice, D., Wirth, R., Xu, Z. Q. and Xia B., 2003, Microstructures, petrofabrics and seismic properties of ultra high-pressure eclogites from Sulu region, China: implications for rheology of subducted continental crust and origin of mantle reflections. Tectonophysics, v. 370, pp. 49–76.

Ji, S. and Martignole, J., 1996, Ductility of garnet as an indicator of extremely high temperature deformation: reply. Journal of Structural Geology, v. 18, pp. 1375–1379.

Jung, W. S., Ree, J. H. and Park, Y., 1999, Non-rotation of garnet porphyroblasts and 3-D inclusion trail data: an example from the Imjingang belt, South Korea. Tectonophysics, v. 307, pp. 381–395.

Karato, S., Wang, Z., Liu, B. and Fujino, K., 1995, Plastic deformation of garnets: Systematics and implications for the rheology of the mantle transition zone. Earth and Planetary Science Letters, v. 130, pp. 13–30.

Kleinschodt, R. and McGrew, A. J., 2000, Garnet plasticity in the lower continental crust: implications for deformation mechanisms based on microstructures and SEM electron channeling pattern analysis. Journal of Structural Geology, v. 22, pp. 795–809.

LeFort, P., 1996, Evolution of the Himalaya, in The Tectonics of Asia, edited by Yin, A. and T. M. Harrison, pp. 95-106, Cambridge University Press, New York.

Liu, Z., Liu, Y. and Zhong, D., 1998, Tectonic framework of the eastern Himalayan syntaxis. Progress in Natural Science v. 8, pp. 366–370.

Mainprice, D., 2004, Crystal preferred orientations of garnet: comparison between numerical simulations and electron back-scattered diffraction (EBSD) measurements in naturally

deformed eclogites. Journal of Structural Geology, v. 26, pp. 2089–2102.

Mezger, K., Essene, E. J. and Halliday, A. N., 1992, Closure temperatures of the Sm-Nd system in metamorphic garnets. Earth and Planetary Science Letters, v. 113, pp. 397–409.

Mezger, K., Hanson, G. N. and Bohlen, S. R., 1989, U-Pb systematics of garnet: Dating the growth of garnet in the Late Archean Pikwitonei granulite domain at Cauchon and Natawahunan Lakes, Manitoba, Canada. Contributions to Mineralogy and Petrolog, v. 101, pp. 136–148.

Passchier, C. W., Trouw, R. A. J., Zwart, H. J. and Vissers, R. L. M., 1992, Porphyroblast rotation: eppur simuove. Journal of Metamorphic Geology, v. 10, pp. 283–294.

Prior, D. J., Wheeller, J., Peruzzo, L., Sqiess, R. and Storey, C., 2002, Some garnet microstructures: an illustration of the potential of orientation maps and misorientation analysis in microstructural studies. Journal of structural geology, v. 24, pp. 999–1011.

Rabier, J. and Garem, H., 1984, Plastic deformation of oxides with garnet structure: deformation of ceramics materials II In: Tressler R E, Bradt R C eds. Materials Science Research. v. 18, pp. 187–198, Plenum Press, New York and London.

Schmidt, N. H. and Olesen, O., 1989, Computer-aided determination of crystal-lattice orientation from electron channeling patterns in the SEM. Canadian Mineralogist, v. 28, pp. 15–22.

Spear, F. S., 1993, Metamorphic Phase equilibria and pressure-temperature-time paths. Washington D C: Mineralogical Society of America, pp. 1–799.

Stallard, A. and Hickey, K., 2001, Shear zone vs folding origin for spiral inclusion trails in the Canton Schist. Journal of Structural Geology, v. 23, pp. 1845–1864.

Steinhardt, C. K., 1989, Lack of porphyroblast rotation in noncoaxially deformed schists from Petrel Cove, South Australia and its implications. Tectonophysics, v. 158, pp. 127–140.

Storey, C. D. and Prior, D. J., 2005, Plastic deformation and recrystallization of garnet: a mechannism to facilitate diffusion creep. Journal of Petrology, v. 46, pp. 2593–2613.

Toshiaki, M. and Sachiyo, M., 1989, Development of snowball structure: numerical simulation of inclusion trails during synkinematic porphyroblast growth in metamorphic rocks. Tectonophysics, v. 170, pp. 141–150.

Vollbrecht, A., Pawlowski, J., Leiss, B, Heinrichsa, T., Seidela, M. and Kronza, A., 2006, Ductile deformation of garnet in mylonitic gneisses from the Münchberg Massif (Germany). Tectonophysics, v. 427, pp. 153–170.

Wadia, D. N., 1931, The syntaxis of the northwest Himalayas: its rocks, tectonics and orogeny. Records of the Geological Survey of India, v. 65, pp. 189–220.

Williams, P. F. and Jiang, D., 1999, Rotating garnets. Journal of Metamorphic Geology, v. 17, pp. 367–378.

Xu, Z. Q., Ji, S. C., Cai, Z. H., Zeng, L. S., Geng, Q. R. and Cao, H., 2012, Kinematics and dynamics of the Namche Barwa Syntaxis, eastern Himalaya: Constraints from deformation, fabrics and geochronology. Gondwana Research, v. 21, pp. 19–36.

Yin, A. and Harrison T. M., 2000, Geologic evolution of the Himalayan-Tibetan orogen, Annual Review of Earth and Planetary Sciences, v. 28, pp. 211–280.

Yin, A., Dubey C. S., Kelty, T. K., Gehrels, G. E., Chou, C. Y., Grove, M. and Lovera, O., 2006, Structural evolution of the Arunachal Himalaya and implications for asymmetric development of the Himalayan orogen, Current Science, v. 90, pp. 195–206.

Zhang, Z. M., Zheng, L. L., Wang, J. L., Zhao, X. D. and Shi, C., 2007, Garnet Pyroxenite in the Namjagbarwa Group-complex in the eastern Himalayan Tectonic Syntaxis, Tibet, China: Evidence for Subduction of the Indian Continent beneath the Eurasian Plate at 80~100 km Depth. Geological Bulletin of China, v. 26, pp. 1–12 (in Chinese with English abstract).

Zhong, D. L. and Ding, L., 1996, The Mechanism for the Tibetan plateau uplift. Science in China (Series D), v. 26 (4), pp. 289–295.